RECONSTRUCTION OF 3-D BURIED OBJECTS FROM ELECTROMAGNETIC DATA RECEIVED BY INACCURATELY POSITIONED RECEIVERS

Hui ZHOU, Takashi TAKENAKA, and Toshiyuki TANAKA

Dept. of Electrical & Electronic Eng., Faculty of Eng., Nagasaki Univ.
1-14 Bunkyo-machi, Nagasaki 852-8521, Japan.
E-mail zhou@net.nagasaki-u.ac.jp

1. Introduction

Ground penetrating radars (GPR) are being applied to detect subsurface structures and targets buried in the ground [1-4]. There are two general ways to detect shallowly buried objects, one is based on image and signal processing [5-9] and the other is on inverse scattering [10-12]. It is not so easy to separate direct wave and reflections from targets if the buried objects are at a shallow depth, particularly when the background media are inhomogeneous and the surface is not flat. An inverse scattering method, which can use total wave fields including direct couplings, reflections or diffractions, may be easy to use in detection of shallowly buried objects.

Forward-backward time-stepping (FBTS) method [10-13] can utilize the whole wave fields. We have discussed it for reconstructing 3-D objects in free space background [13] and in homogeneous half space with flat surface [10]. In this paper we apply this inversion technique to rebuild a 3-D mine shallowly buried in homogeneous half space. We focus the subject of this paper on the influence of inaccurate positions of receivers, i.e., the positions of receivers used for observed data and guessed data may be different. The deviations of receiving positions are random. This paper discusses the derivation of the FBTS method and several numerical examples.

2. The FBTS method

Maxwell's equation is expressed as

$$L\mathbf{v} = \mathbf{j}, \tag{1}$$

where $\mathbf{v} = \left(E_x\ E_y\ E_z\ \eta H_x\ \eta H_y\ \eta H_z\right)^t$, $\mathbf{j} = \left(\eta J_x\ \eta J_y\ \eta J_z\ 0\ \ 0\ \ 0\right)^t$, E_x, E_y, E_z and H_x, H_y, H_z are components of electric and magnetic fields, η is the impedance in free space, and the superscript t represents transpose. The differential operator L is given by

$$L \equiv \overline{A}\frac{\partial}{\partial x} + \overline{B}\frac{\partial}{\partial y} + \overline{C}\frac{\partial}{\partial z} - \overline{F}\frac{\partial}{\partial (ct)} - \overline{G}, \tag{2}$$

$$\overline{F} = \begin{pmatrix} \varepsilon_r \overline{I} & \mathbf{0} \\ \mathbf{0} & \mu_r \overline{I} \end{pmatrix},\ \ \overline{G} = \begin{pmatrix} \eta\sigma \overline{I} & \mathbf{0} \\ \mathbf{0} & \mathbf{0} \end{pmatrix}, \tag{3}$$

where $\overline{A}$, $\overline{B}$, $\overline{C}$ are 6×6 constant matrixes, c is the velocity of light in free space, ε_r is relative permittivity, μ_r is relative permeability, and σ is conductivity, $\overline{I}$ is a 3×3 unit matrix.

Suppose that in a homogeneous background there is an inhomogeneous object. Ideal dipole transmitters in the y-direction at $\mathbf{r}_m^t$ $(m = 1, 2, \cdots, M)$ illuminate the object with a current pulse $J(t)$ in the y-direction. For each illumination the y-component of time-domain electric field data are collected by ideal dipoles in the y-direction at $\mathbf{r}_n^r$ $(n = 1, 2, \cdots, N)$. The distributions of the electrical parameters $\mathbf{p} = \left(\varepsilon_r\ \mu_r\ \eta\sigma\right)^t$ are reconstructed from the received data by minimizing the functional

$$F(\mathbf{p}) = \int_0^{cT} \sum_{m=1}^{M}\sum_{n=1}^{N} K_{mn}(t) \left| E_{ym}(\mathbf{p}; \mathbf{r}_n^r, t) - \tilde{E}_{ym}(\mathbf{r}_n^r, t) \right|^2 d(ct), \tag{4}$$

where $\tilde{E}_{ym}(\mathbf{r}_n^r, t)$ is the observed y-component of electric field at $\mathbf{r}_n^r$ under the excitation by the source $\mathbf{j}_m$, $E_{ym}(\mathbf{p}; \mathbf{r}_n^r, t)$ is the calculated y-component of electric field for guessed parameters $\mathbf{p}$,

ISBN: 4-88552-206-4 C3055©IEICE

$K_{mn}(t)$ is a continuous non-negative weighting function with a value of 0 at $t = T$, T is the duration of observed data.

The Fréchet differential of the functional is

$$F'(\mathbf{p})\delta\mathbf{p} = 2\int_0^{cT}\sum_{m=1}^{M}\sum_{n=1}^{N} u_m(\mathbf{p};\mathbf{r}_n^r,t)\delta E_{ym}(\mathbf{p};\mathbf{r}_n^r,t)d(ct)\,, \tag{5}$$

where $u_m(\mathbf{p};\mathbf{r}_n^r,t)$ is the weighted residual, $\delta E_{ym}(\mathbf{p};\mathbf{r}_n^r,t)$ is the y-component of $\delta\mathbf{v}_m(\mathbf{p};\mathbf{r}_n^r,t)$ satisfying Eqs.(6) and (7)

$$L(\delta\mathbf{v}_m) = \delta\overline{F}\frac{\partial\mathbf{v}_m}{\partial(ct)} + \delta\overline{G}\mathbf{v}_m\,, \tag{6}$$

$$\delta\mathbf{v}_m(\mathbf{p};\mathbf{r},0) = \mathbf{0}\,, \tag{7}$$

where $\delta\overline{F}$ and $\delta\overline{G}$ are the variations of $\overline{F}$ and $\overline{G}$.

To express the gradient of $F(\mathbf{p})$ with respect to $\mathbf{p}$ explicitly, an adjoint operator L^* is introduced. It is defined as

$$L^* = -\overline{A}\frac{\partial}{\partial x} - \overline{B}\frac{\partial}{\partial y} - \overline{C}\frac{\partial}{\partial z} + \overline{F}\frac{\partial}{\partial(ct)} - \overline{G}\,. \tag{8}$$

By using an adjoint field $\mathbf{w}_{mn}(\mathbf{p};\mathbf{r},t)$ satisfying

$$L^*\mathbf{w}_{mn} = \mathbf{i}_y u_m(\mathbf{p};\mathbf{r}_n^r,t)\delta(\mathbf{r}-\mathbf{r}_n^r)\,, \tag{9}$$

$$\mathbf{w}_{mn}(\mathbf{p};\mathbf{r},T) = \mathbf{0}\,, \tag{10}$$

and considering Eqs.(6) and (9), we can express the Fréchet differential (5) as the form of

$$F'(\mathbf{p})\delta\mathbf{p} = \langle g_\varepsilon, \delta\varepsilon_r\rangle + \langle g_\mu, \delta\mu_r\rangle + \langle g_{\eta\sigma}, \delta(\eta\sigma)\rangle\,. \tag{11}$$

Finally, the gradient g_ε, g_μ, $g_{\eta\sigma}$ of $F(\mathbf{p})$ with respect to ε_r, μ_r and $\eta\sigma$ are given explicitly, for example

$$g_\varepsilon = 2\int_0^{cT}\sum_{m=1}^{M}\sum_{i=1}^{3} w_m^i(\mathbf{p};\mathbf{r},t)\frac{\partial v_{im}(\mathbf{p};\mathbf{r},t)}{\partial(ct)}\,d(ct)\,, \tag{12}$$

where $w_m^i(\mathbf{p};\mathbf{r},t) = \sum_{n=1}^{N} w_{mn}^i(\mathbf{p};\mathbf{r},t)$, $w_{mn}^i(\mathbf{p};\mathbf{r},t)$ is the ith component of $\mathbf{w}_{mn}(\mathbf{p};\mathbf{r},t)$.

3. Numerical examples

The configuration of transmitters and receivers is shown in Fig. 1. Transmitting and receiving antennas, which are assumed to be ideal dipoles orientated in the $y-$direction, are set on a plane 3.6 cm above the ground surface. The number of transmitters is 16, and that of receivers is 64. The transmitter interval is 9.6 cm, the receiver interval is 4.8 cm, for accurate positioning, in horizontal directions. Incident current pulse is expressed as

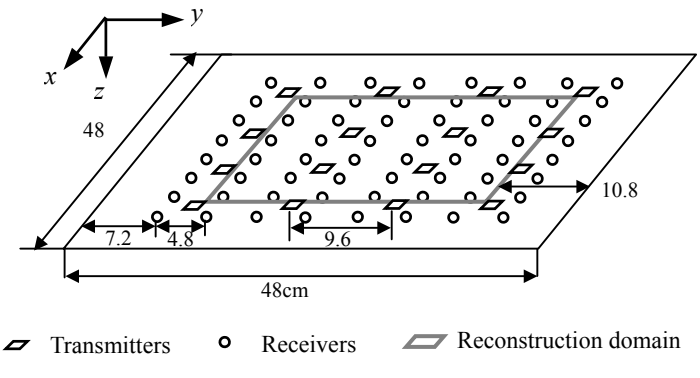

Fig.1 Configuration of transmitters and receivers.

$$J(t) = \frac{d^3}{dt^3}\exp\left[-\alpha^2(t-\tau)^2\right], \tag{13}$$

where $\tau = \beta\Delta t$, $\alpha = 4/\tau$, $\beta = 145$, Δt is time step. The highest frequency of the incident pulse is 1.0 GHz. For both forward and backward calculations using FDTD, spatial and time steps are $\Delta x = \Delta y = \Delta z = 1.2$ cm and $\Delta t = 22.65$ ps, and the measurement duration is $T = 550\Delta t$.

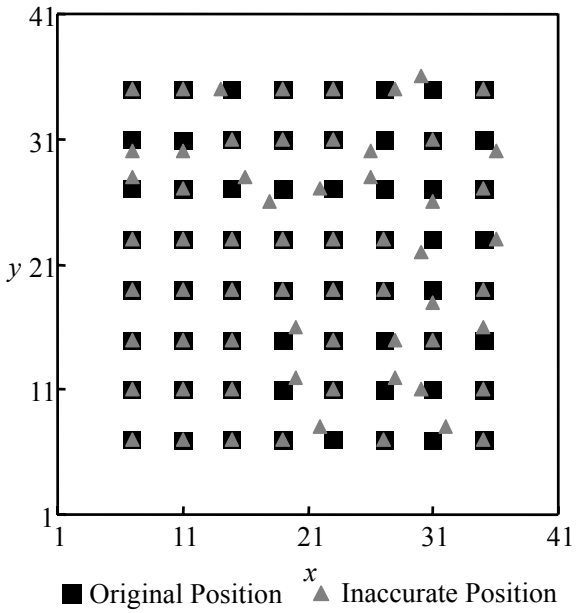

Fig.2 Receiver positions for the first transmitter.

The relative permittivity of the soil is 6 and a cylindrical mine of relative permittivity 4 is buried 3.6 cm beneath the surface. The mine is 10 cm in height and 15 cm in diameter. The FDTD space is a cube with a side length of 42 cells, and the reconstruction area is the region between the 10th-32nd, 10th-32nd, 8th-25th grid points in the x, y, and z-directions, respectively. The surface is located at grid point 8 in the z-direction. The projection of the reconstruction region on the transmitter-receiver plane is shown in Fig. 1 as the area surrounded by the gray rectangular.

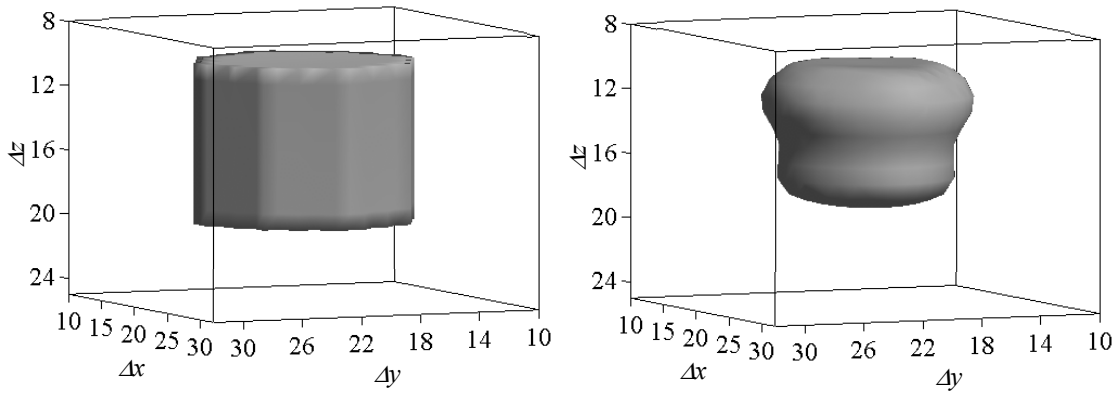

Fig.3 Three-dimensional profile of relative permittivity of the reconstruction region: (a) original profile, (b) reconstructed result from noise-free data after 20 iterations.

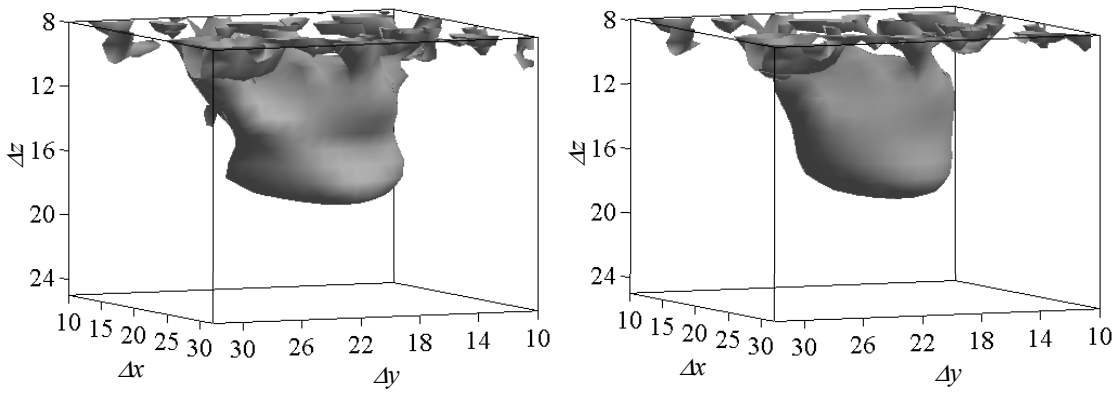

Fig.4 3-D profile of relative permittivity of the reconstruction region after 20 iterations:
(a) reconstructed result from noisy and inaccurate positioning data,
(b) same as (a) but by applying filters.

The initial guess of relative permittivity of the reconstruction region is that of the background. Fig.2 shows a sample of the original and inaccurate positions of receivers for a transmitter used in simulation of "observed" data and calculated data from guessed model parameters. Fig. 3(a) shows the original profile of relative permittivity of the reconstruction region. Fig. 3(b) is the reconstructed result using position error-free and noise-free data after 20 iterations. Fig. 4(a) is the reconstructed result using noisy data with signal to noise ratio of 20 dB, and inaccurate receiver positions. Fig. 4(b) is the reconstructed result using inaccurate positioning and noisy data with the same signal to noise ratio and by applying three filters during the iterations. From Figs. 3 and 4 we learn that although the reconstructed size of the mine after 20 iterations is smaller than the true one, the existence of a mine-like object in the soil can be clearly confirmed.

4. Conclusions

The reconstruction of a 3-D mine buried in soil has been succeeded using synthetic noise-free and noisy data and inaccurate positioning data in the time-domain. After 20 iterations, it can be confirmed whether there is something different from the soil.

5. Acknowledgements

This research is supported by Ministry of Culture and Science, Japan (C)(2)15560361, and Japan Science and Technology (JST) Corporation.

References

[1] Zhou, H., and Sato, M., "Archaeological application of ground penetrating radar to Sendai Castle," *Archaeological Prospection*, **Vol. 8**, 2001, pp.1–11.

[2] Zhou, H., and Sato, M., "Application of vertical radar profiling technique to Sendai Castle," *Geophysics*, **Vol. 65**, 2000, pp.533–539.

[3] Xu, X., Miller, E. L., Rappaport, C. M., and Sower, G. D., "Statistical method to detect subsurface objects using array ground-penetrating radar data," *IEEE Trans Geosci Remote Sensing*, **Vol. 40**, 2002, pp.963–976.

[4] Morrow, I. L., and Genderen, P. van, "Effective imaging of buried dielectric objects," *IEEE Trans Geosci Remote Sensing*, **Vol. 40**, 2002, pp.943–949.

[5] Gader, P. D., Mystkowski, M., and Zhao, Y., "Landmine detection with ground penetrating radar using hidden Markov models," *IEEE Trans Geosci Remote Sensing*, **Vol. 39**, 2001, pp.1231–1244.

[6] Sagues, L., Lopez-Sanchez, J.M., Fortuny, J., et al., "Polarimetric radar interferometry for improved mine detection and surface clutter rejection," *IEEE Trans Geosci Remote Sensing*, **Vol. 39**, 2001, pp.1271–1278.

[7] Xu, Y., Narayanan, R. M., Xu, X., and Curtis, J. O., "Polarimetric processing of coherent random noise radar data for buried object detection," *IEEE Trans Geosci Remote Sensing*, **Vol. 39**, 2001, pp.467–478.

[8] A. van der Merwe, and Gupta I. J., "A novel signal processing technique for clutter reduction in GPR measurements of small, shallow land mines," *IEEE Trans Geosci Remote Sensing*, **Vol. 38**, 2000, pp.2627–2637.

[9] O'Neill, K., "Radar sensing of thin surface layers and near-surface buried objects," *IEEE Trans Geosci Remote Sensing*, **Vol. 38**, 2000, pp.480–495.

[10] Zhou, H., Takenaka T., and Tanaka T., "Three-dimensional reconstruction of shallowly buried mine using time-domain data," *Microwave and Optical Technology Letters*, **Vol.39** (4), 2003, pp.276-280.

[11] Meincke P. "Linear GPR inverseion for lossy soil and a planar air-soil nterface," *IEEE Trans Geosci Remote Sensing*, **Vol. 39**, 2001, pp.2713–2721.

[12] Bermani E., Boni A., Caorsi, S., et al., "An innovative real-time technique for buried object detection," *IEEE Trans Geosci Remote Sensing*, **Vol. 41**, 2003, pp.927–931.

[13] Takenaka T., Zhou, H., and Tanaka T., "Inverse scattering for a three-dimensional object in the time domain," *Journal of Optical Society of America A* **Vol.20** (10), 2003, pp. 1867-1874.